Vision-Based Force Measurement

Michael A. Greminger and Bradley J. Nelson, *Member*, *IEEE*

Abstract—This paper demonstrates a method to visually measure the force distribution applied to a linearly elastic object using the contour data in an image. The force measurement is accomplished by making use of the result from linear elasticity that the displacement field of the contour of a linearly elastic object is sufficient to completely recover the force distribution applied to the object. This result leads naturally to a deformable template matching approach where the template is deformed according to the governing equations of linear elasticity. An energy minimization method is used to match the template to the contour data in the image. This technique of visually measuring forces we refer to as vision-based force measurement (VBFM). VBFM has the potential to increase the robustness and reliability of micromanipulation and biomanipulation tasks where force sensing is essential for success. The effectiveness of VBFM is demonstrated for both a microcantilever beam and a microgripper. A sensor resolution of less than +/- 3 nN for the microcantilever and +/- 3 mN for the microgripper was achieved using VBFM. Performance optimizations for the energy minimization problem are also discussed that make this algorithm feasible for real-time applications.

Index Terms—Force measurement, deformable templates, elasticity, nonrigid tracking.

1 Introduction

Microassembly is becoming increasingly important because it enables the creation of MEMS devices with greater functionality. Through an assembly process, MEMS devices can be created with three-dimensional features and can consist of structures created by incompatible microfabrication processes. Force sensing is important for microassembly because the objects involved are often fragile. Force sensing is also essential for biomanipulation where the biological cells and tissues being handled are easily damaged. Currently, force measurement at the microscale is usually done using laser-based optical techniques [10] or using piezoresistive material embedded in an elastic part [14]. Both of the methods are difficult to implement because they require a specially designed elastic part. For example, a laser-based optical force sensor requires precise alignment of laser optics with respect to the elastic part and a piezoresistive force sensor requires that a piezoresistive layer be embedded within the part during its manufacture. Vision-based force measurement (VBFM) has the advantage that it can be used with existing elastic parts. It also has the advantage that it makes use of the microscope optics and cameras that are already present in a micromanipulation or biomanipulation workstation.

This paper describes a deformable template matching approach that is used to recover the force applied to an elastic object, where the template deforms according the governing equations of elasticity. The deformable template registers to the Canny edge image [1] of a deformed object using an energy minimization approach. Various optimizations techniques are applied to the energy minimization that provide the potential for using VBFM in real-time applications.

The use of elastic models is well established in computer vision. In 1987, Kass et al. [6] proposed a method to track contours in an image using a 2D elastic model called a snake. These snakes had elastic properties and were attracted to edge features within the image. Metaxas [8] used 3D meshes with physics-based elastic properties to track both rigid and nonrigid objects. Yuille et al. [19] used a deformable template matching algorithm to track facial features. These methods use elastic models as a tool to locate objects within a scene, while the approach described in this paper uses elastic models to extract force information from an image.

Prior work exists in which elastic models are used to derive force or material property information from images. Tsap et al. [15] proposed a method to use nonlinear finite element modeling (FEM) to track nonrigid objects in order to detect the differences in elasticity between normal and abnormal skin. They also discussed how their method could be used for force recovery. Kaneko et al. [5] presented a tactile sensor that was able to measure forces visually; however, their algorithm was limited to wire shaped objects. There has also been work in force measurements at micro and nanoscales using computer vision. Wang et al. [17] used Finite Element Modeling (FEM) techniques to derive the forces that are applied to deformable microparts. Their method is limited by the need to track each FEM mesh point in the image. Danuser and Mazza [2] proposed the use of statistical techniques along with deformable templates to track very small displacements. They applied their technique to the measurement of strain in a microbar under tension. Dong et al. [3] monitored the tip deflection of an AFM cantilever beam in order to obtain the material properties of multiwalled carbon nanotubes. The force measurement algorithm presented here is unique in using contour data alone, therefore, no feature tracking is required and the method can be generalized to elastic objects with different geometries.

- *M.A. Greminger is with the Department of Mechanical Engineering, University of Minnesota, Minneapolis, MN 55455. E-mail: grem@me.umn.edu.*
- *B.J. Nelson is with the Institute of Robotics and Intelligent Systems, Swiss Federal Institute of Technology (ETH), CH-8092 Zurich, Switzerland. E-mail: brad.nelson@iris.mavt.ethz.ch.*

Manuscript received 18 June 2002; revised 12 Sept. 2003; accepted 15 Sept. 2003.
Recommended for acceptance by R. Sharma.
For information on obtaining reprints of this article, please send e-mail to: tpami@computer.org, and reference IEEECS Log Number 116791.

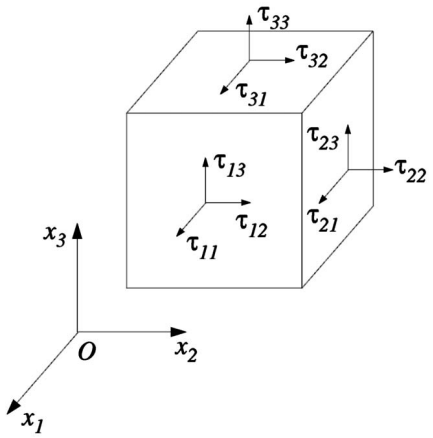

Fig. 1. Cube in three-dimensional state of stress.

This paper is organized as follows: Section 2 formulates the elasticity problem and concludes by showing how the Dirichlet to Neumann map can be used to recover the force distribution applied to an elastic object using the displacement field of the contour. The problem of recovering the displacement field of the contour of an elastic object is discussed in Section 3, where it is shown that the recovery of the contour displacement field can be solved using deformable templates. Section 4 formulates the deformable template matching algorithm for a cantilever beam. The application of VBFM to a microgripper device is discussed in Section 5. Section 6 presents performance optimizations used to make the template matching process more efficient. A concluding discussion is given in Section 7.

2 Linear Elasticity Theory

In this paper, we consider deformable objects that are linearly elastic. Linear elasticity theory assumes that the object's strains are infinitesimal and that the object's stress-strain relationship is linear. Both of these assumptions are satisfied for the materials to be considered here: silicon and steel. Both silicon and steel exhibit a linear stress-strain relationship for a large working range and both will fail if subject to strains that are not infinitesimal. We also assume a state of two-dimensional stress within the object that is referred to as plane stress.

2.1 The Formulation of the Plane Stress Elasticity Problem

The plane stress assumption assumes a state of stress where there is no stress in the x_3 direction of an object. Therefore, the stress components τ_{13}, τ_{23}, and τ_{33} will have a value of zero (see Fig. 1). The remaining stress components, τ_{11}, τ_{22}, and τ_{12}, are functions of x_1 and x_2 only. Consider the bounded two-dimensional domain R shown in Fig. 2. It is assumed that R is defined such that the divergence theorem applies. Two-dimensional domains where the divergence theorem applies are those that are bounded by a finite number of piecewise smooth curves [4] and are known as normal domains. The elastic body defined by R is governed by the equations of elasticity which are simplified for the plane stress case. The equations of elasticity can be expressed in terms of displacements $u(x)$ by [12]:

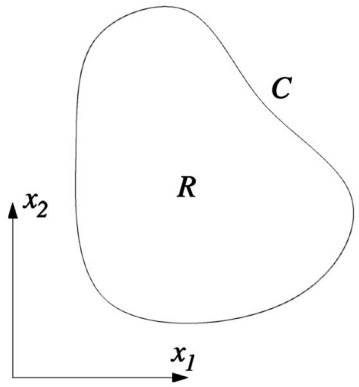

Fig. 2. Elastic body R and its associated contour C.

$$\mu\nabla^2 u_\alpha + \mu\left(\frac{1+\nu}{1-\nu}\right)\frac{\partial}{\partial x_\alpha}\left(\frac{\partial u_1}{\partial x_1}+\frac{\partial u_2}{\partial x_2}\right)+F_\alpha = 0, \quad (1)$$

where $\alpha = 1, 2$, μ is the shear modulus, and ν is the Poisson's ratio. The material properties of an isotropic, elastic material are completely defined by the shear modulus and the Poisson's ratio.

The boundary conditions for the elasticity problem can be expressed as a prescribed displacement vector f_i on the contour C, known as a Dirichlet boundary condition:

$$u_i|_C = f_i \quad (2)$$

or a prescribed traction vector T_i on C, known as a Neumann boundary condition:

$$\tau_{ij}n_j|_C = T_i, \quad (3)$$

where n_j is the outward unit normal of C and the stress tensor τ_{ij} can be expressed in terms of displacements by [12]:

$$\tau_{11} = \frac{2\lambda\mu}{\lambda+2\mu}\left(\frac{\partial u_1}{\partial x_1}+\frac{\partial u_2}{\partial x_2}\right)+2\mu\frac{\partial u_1}{\partial x_1}, \quad (4)$$

$$\tau_{22} = \frac{2\lambda\mu}{\lambda+2\mu}\left(\frac{\partial u_1}{\partial x_1}+\frac{\partial u_2}{\partial x_2}\right)+2\mu\frac{\partial u_2}{\partial x_2}, \quad (5)$$

$$\tau_{12} = \mu\left(\frac{\partial u_1}{\partial x_2}+\frac{\partial u_2}{\partial x_1}\right), \quad (6)$$

$$\tau_{13} = \tau_{23} = \tau_{33} = 0. \quad (7)$$

The traction vector is the force per unit length applied to the contour of the object. It is assumed throughout this discussion that f_i and T_i have piecewise continuous derivatives.

2.2 The Dirichlet to Neumann Map

The Dirichlet to Neumann map Λ [9], [13] is a mapping from the surface displacements f_i to the surface tractions T_i and can be expressed as:

$$\Lambda(f_i) = \tau_{ij}n_j|_C = T_i. \quad (8)$$

In order for Λ to be defined, it is necessary that for each f_i there exists a unique T_i. The existence and uniqueness theorems of linear elasticity are sufficient to show that the Dirichlet to Neumann map does exist. The uniqueness theorem for the Dirichlet plane stress problem is due to Kirchoff [7].

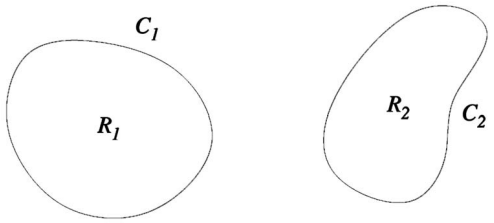

Fig. 3. Undeformed contour C_1 and deformed contour C_2.

Kirchoff's proof shows that the solution to the Dirichlet problem is unique as long as the following conditions on the shear modulus and Poisson's ratio are satisfied:

$$\mu \neq 0 \quad -1 < \nu < \frac{1}{2}, \tag{9}$$

which are satisfied for the materials being considered. The existence of solutions for the Dirichlet plane stress problem can also be shown [12]. The existence of the Dirichlet to Neumann map shows that the traction distribution on the contour of a linearly elastic body can be uniquely determined if the displacement field of its contour is known.

In general, the existence of the Dirichlet to Neumann map cannot be proven for nonlinear problems. However, the concept of the Dirichlet to Neumann map can be applied to nonlinear problems where the mapping can often be computed using numerical modeling techniques.

3 Recovery of Boundary Displacement Field from Contour Data

The vision-based force measurement problem is thus reduced to that of finding the displacement field of the contour of an object. Fig. 3 shows an undeformed contour C_1 along with a deformed contour C_2. In general, the problem of determining the displacement field that leads to the deformed contour C_2 does not have a unique solution. Fig. 4 illustrates this point by showing how two distinct displacement fields can lead to two identical deformed contours, C_2 and C_3. Three points, P_1, P_2, and P_3, are shown on the undeformed contour C_1 as well as on the deformed contours C_2 and C_3. Experience with elastic objects suggests that the displacement field that created the contour C_2 is the correct one; however, both displacement fields are equally valid.

In order to find a unique displacement field for a given deformed contour, it is necessary to make some assumptions

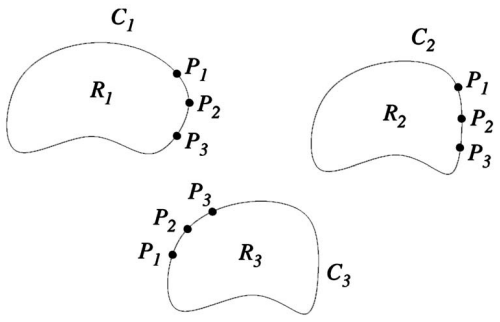

Fig. 4. Illustration of two distinct displacement fields that lead to identical deformed contours, C_2 and C_3.

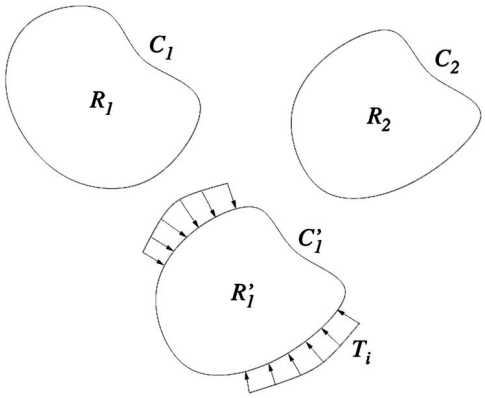

Fig. 5. The contour C_1 is perturbed by the traction distribution T_i so that it matches the deformed contour C_2.

about the object that is being deformed. We assume that it behaves according to (1) and that the strain components are infinitesimal. With the assumption of infinitesimal strains it becomes clear that the displacement field that led to contour C_3 is not physically possible because it would require large strain values. Since the strains are assumed to be small, the deformed contour will not differ much from the undeformed contour. With these assumptions in mind, a logical way to recover the displacement field is to perturb the undeformed contour C_1 (see Fig. 5) by small amounts until it matches the deformed contour C_2. The undeformed contour will be perturbed by assuming a traction distribution T_i and then deforming the contour according to (1). Fig. 5 shows a perturbed contour C_1', with a traction distribution T_i applied to it, which matches the deformed contour C_2.

The perturbation approach just described can be implemented with a deformable template matching algorithm where the undeformed template is the undeformed contour of the object, C_1, and the template is perturbed by a traction distribution T_i according to the governing equations of elasticity to obtain the deformed contour C_1'. If the elastic model used to deform the template accurately models the elastic object shown in the image, the solution to the Dirichlet to Neumann Map is given by the traction distribution, T_i, applied to deform the template. Therefore, the Dirichlet to Neumann map can be evaluated for a particular deformed object through the use of deformable template matching provided that the template is deformed according the equations of elasticity. The following section demonstrates how this deformable template matching technique can be applied to a cantilever beam.

4 Force Recovery with Deformable Templates

As mentioned above, the Dirichlet to Neumann map can be evaluated by a deformable template matching technique. The first object tested with this type of template was a silicon cantilever beam 450 μm long. An image of the cantilever beam is shown in Fig. 6. The beam is of a type manufactured using standard microfabrication techniques and used in many types of atomic force measurement approaches.

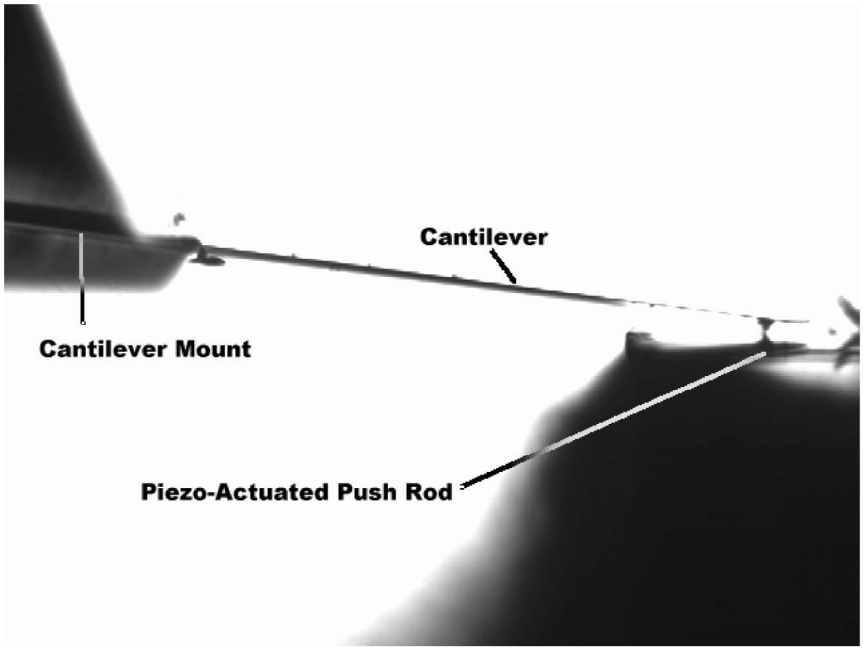

Fig. 6. Image of microcantilever beam.

The deformable template is registered to a binary edge image [1] using a least square error measure. The template is represented by a list of 2D vertices r^i and the edge pixels in the current image are represented by the list of 2D vertices w^i. The registration algorithm minimizes the distance squared between the transformed template vertices $r^{i'}$ and the nearest image edge vertices w^i where the template vertices are transformed by a elastic transformation and a rigid body transformation.

4.1 The Rigid Body Portion of Template Matching Algorithm

The rigid body portion of the transformation of the template vertices is simply an affine transformation given by:

$$r^{i'} = A(r^i), \tag{10}$$

where A is defined by

$$A(r^i) = X + \begin{bmatrix} \cos\theta & -\sin\theta \\ \sin\theta & \cos\theta \end{bmatrix} r^i, \tag{11}$$

where θ is the rotation of the template about its origin and X is the translation vector.

The error function is given by:

$$E(\theta, X) = \sum_{i=1}^{N} \|r^{i'} - w^i\|^2, \tag{12}$$

where $r^{i'}$ is the position vector of the th edge pixel of the template transformed by (10), w^i is the position vector of the edge pixel in the image that is closest to the point $r^{i'}$, and N is the number of edge pixels in the template. This error function sums the distance squared between each of the template edge pixels and the closest edge pixel on the image. Since the transformed position vector $r^{i'}$ is related to the original position vector r^i by the affine transformation A, E is a function of θ and X. By minimizing (12), the values of θ and X that best match the image in a least squares sense can be determined.

The error function given by (12) is minimized by a first-order multivariable minimization technique called the Broydon-Fletcher-Goldfarb-Shanno (BFGS) method [16].

4.2 Incorporating Force into the Template Matching Algorithm

Minimizing (12) will determine the rigid body motion of the object. The nonrigid motion of the template will be modeled using (1). For the cantilever beam, the Bernoulli-Euler law is assumed to apply [12]. The Bernoulli-Euler law can be used to simplify (1) and leads to the following displacement solution for the cantilever beam shown in Fig. 7a:

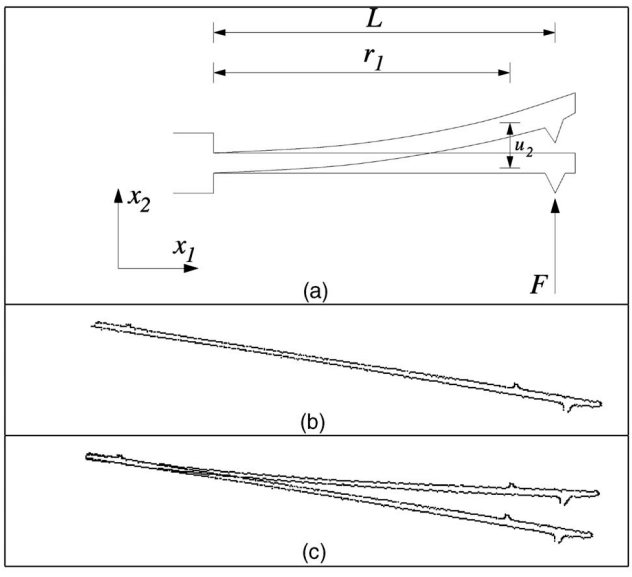

Fig. 7. Deformable cantilever template.

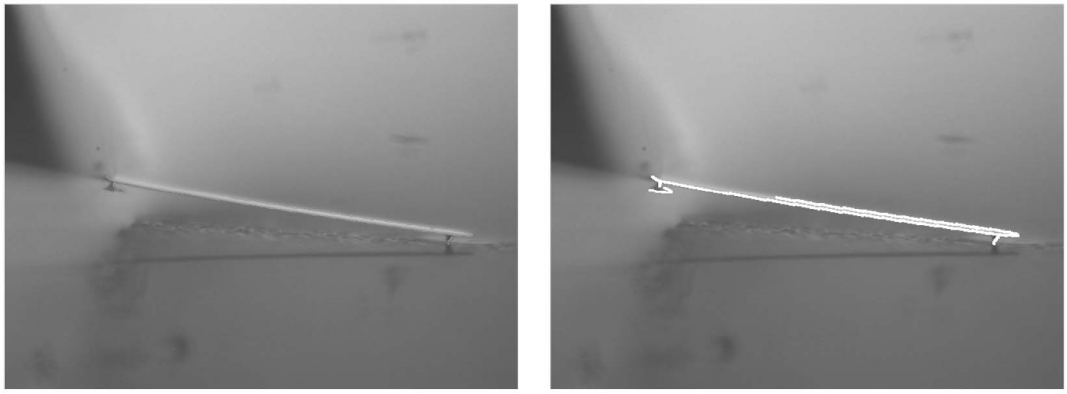

(a) (b)

Fig. 8. (a) Deflected cantilever. (b) The template matched to the deflected cantilever.

$$\begin{bmatrix} u_1 \\ u_2 \end{bmatrix} = \begin{bmatrix} 0 \\ \frac{Fr_1^2}{6EI}(3L - r_1) \end{bmatrix}, \tag{13}$$

where F is the force being applied to the cantilever, L is the length of the cantilever, E is the modulus of elasticity of the cantilever, and I is the moment of inertia of the cantilever's cross section.

Next, it is necessary to apply this displacement field to the cantilever template. It can be seen from (13) that the x_1 component of the template points will remain unchanged. It should also be noted that, if a template point's x_1 component is less than zero, then the point will not be transformed. If a template point's x_1 component is between zero and L, then the point will be translated in the x_2 direction by u_2 in (13). Points with an x_1 component greater than L will be translated in the x_2 direction, but the equation will be different from (13) because the radius of curvature of the cantilever becomes infinite for $r_1 > L$. Once all of the template points are translated appropriately, then (10) can be applied to the new template points to transform them to the image coordinate system. This is shown by the following equations:

$$r' = A(r) \quad \text{for} \quad (r_1 < 0), \tag{14}$$

$$r' = A\left(\begin{bmatrix} r_1 \\ r_2 \end{bmatrix} + \begin{bmatrix} 0 \\ \frac{Fr_1^2}{6EI}(3L - r_1) \end{bmatrix}\right) \quad \text{for} \quad (0 \le r_1 < L), \tag{15}$$

$$r' = A\left(\begin{bmatrix} r_1 \\ r_2 \end{bmatrix} + \begin{bmatrix} 0 \\ \frac{FL^2}{6EI}(3r_1 - L) \end{bmatrix}\right) \quad \text{for} \quad (L \le r_1). \tag{16}$$

When the error function (12) is used with a template transformed by (14) through (16), the error function becomes a function of one additional variable, the force F applied to the template. This is shown by the following error function:

$$E(\theta, X, F) = \sum_{i=1}^{N} \|r^{i\prime} - w^i\|^2. \tag{17}$$

When this error function is minimized, in addition to giving the position of the cantilever within the image, the force that is being applied to the cantilever can be obtained. Fig. 7b shows the undeformed cantilever template that was obtained from a

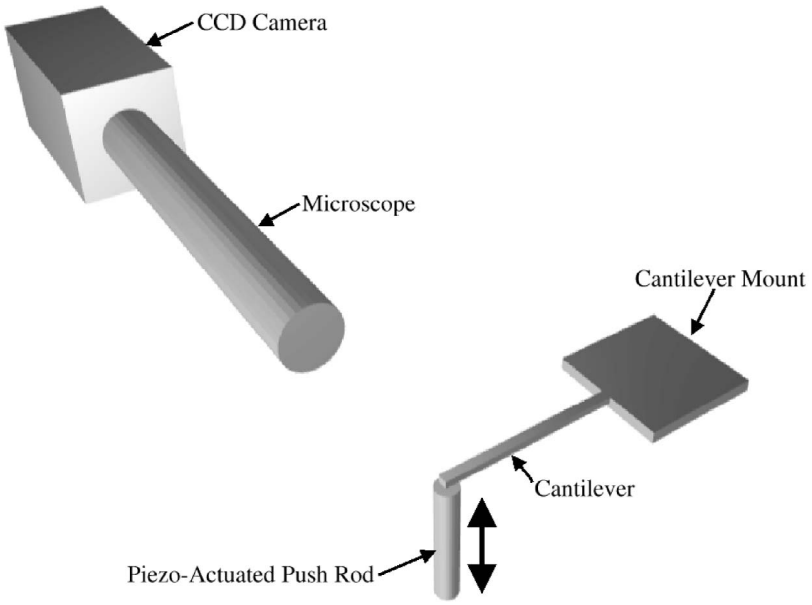

Fig. 9. Force sensing system configuration.

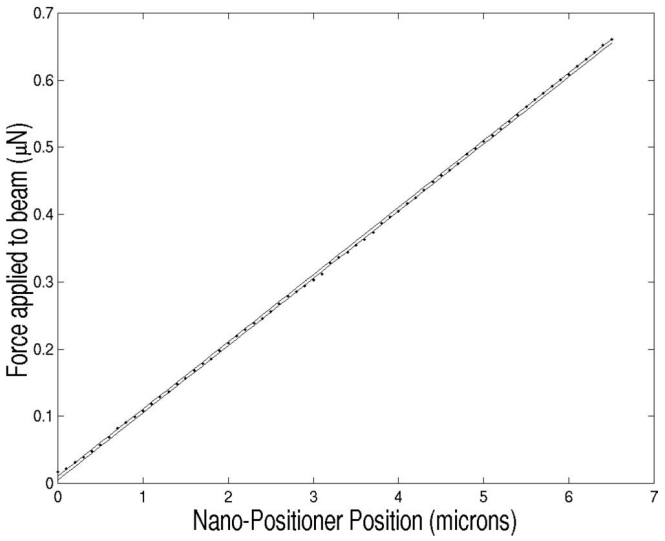

Fig. 10. Calibration plot for cantilever force sensor with 20x objective lens.

Canny edge image of the cantilever. Fig. 7c shows a deformed template along with the undeformed template. Fig. 8a shows an image of a deflected cantilever beam and Fig. 8b shows a cantilever template matched to the image.

4.3 Experimental Setup

A diagram of the force sensing system used with the cantilever beam is shown in Fig. 9. The cantilever beam is an AFM probe tip 450 μm long with a spring constant of approximately 0.1 N/m. A known displacement is applied to the cantilever beam using a three DOF piezo-actuated nanopositioner from Queensgate with subnanometer positioning resolution. A microscope mounted with a CCD camera is used to obtain an image of the cantilever. A video capture card then digitizes this image. An image captured from the CCD camera is shown in Fig. 6.

4.4 Cantilever Results

To evaluate the performance of the VBFM algorithm, a known displacement was applied to the cantilever beam using a Queensgate nanopositioner. These displacement inputs were used to calibrate the force measurement system. Fig. 10 shows a force versus applied displacement plot. The 1 σ prediction intervals are shown on the plot. The maximum 1 σ prediction value for the force measurements is +/- 2.85 nN. The system was tested with both a 10x and a 20x objective lens. Table 1 summarizes the performance of the force sensor with both the 10x objective lens and the 20x objective lens.

5 Algorithm Applied to Microgripper

The methods presented in this paper can be applied to more complex objects. In order to use this algorithm, it is necessary to perturb the undeformed contour of the elastic object as was done for the case of the cantilever beam. This deformed contour field might be obtained in a closed form solution, such as was done for the cantilever in (13) or through numerical methods such as FEM. Once the deformed contour is determined, it can be applied to the template in a manner analogous to (14) through (16) where each template point is displaced as a function of its position in the elastic body and the traction distribution applied to the body.

Fig. 11a shows a microgripper developed by Yang et al. which is used for a specific microassembly task [18]. The gripper is cut by microwire electrodischarge machining (EDM) from spring steel 254 μm thick. A tube slides over the gripper to force the jaws of the gripper together in order to grasp an object. When this gripper is used for an assembly task, it is important to measure the gripping force that the gripper applies to the object being held in order to ensure a stable grasp is achieved and to avoid damage to the object being grasped.

5.1 Modeling of the Microgripper

Each jaw of the gripper can be modeled as a cantilever beam. Fig. 11c shows the deflection model, where D is the displacement of the jaw due to the clamping tube making contact with the gripper, F is the force applied to the object being held, and u is the displacement of the jaw at a position x along its length. D is a function of the tube position, L_2, and can be written as:

$$D = L_2 \sin\beta - r\cos\beta, \tag{18}$$

where r is the inner radius of the clamping tube. Because the tube forces the gripper jaw to deflect, there is a reaction force R applied to the tube by the jaw. We solve for the displacement field, u, as a function of x, F, and L_2 in order to create the deformable gripper template. In order to solve for u, it is first necessary to solve for the reaction force of the gripper jaw on the clamping tube, R. The displacement D applied to the gripper is a redundant constraint on the cantilever beam, so the reaction force R can be solved for by using the beam equation with the constraint that the displacement must be D at the location where the tube comes into contact with the gripper jaw. Once the reaction force R is known, it is straightforward to calculate the displacement field, u, of the jaw using the Bernoulli-Euler law. The use of the Bernoulli-Euler law was justified through simulations

TABLE 1
Summary of Results for Visual Force Sensor Applied to a Cantilever Beam

Magnification	NA	Rayleigh Limit (μm)	Pixel Size (μm)	Deflection Prediction Uncertainty (nm)	Force Prediction Uncertainty (nN)
10x	.28	1.000	1.050	1σ 88.7	8.87
				2σ 180.5	18.05
				3σ 276.5	27.65
20x	.42	.700	.530	1σ 28.5	2.85
				2σ 58.0	5.80
				3σ 88.7	8.87

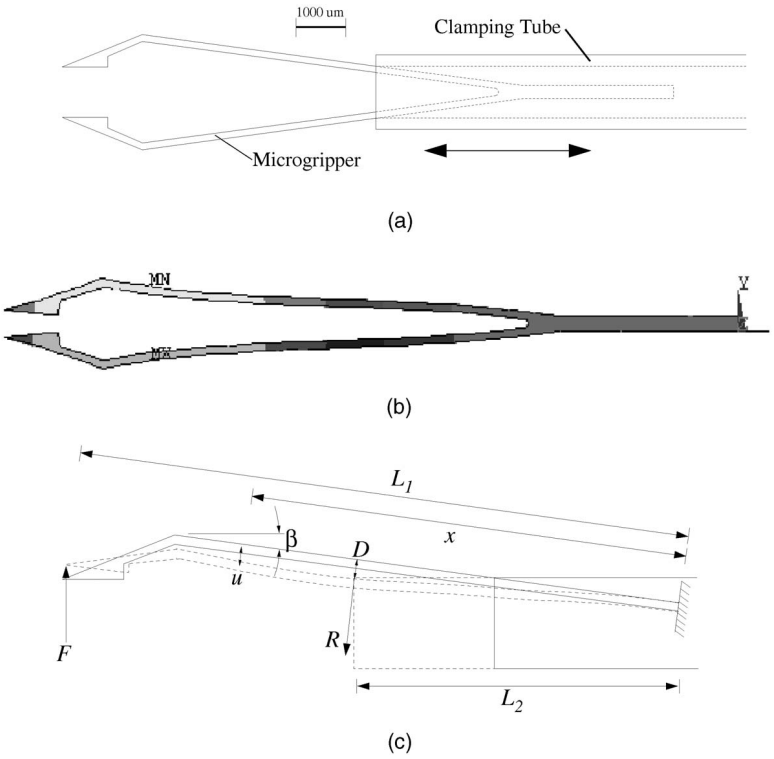

Fig. 11. (a) Microgripper manipulator, (b) gripper ANSYS model, and (c) gripper jaw deflection model.

with ANSYS. The deformed ANSYS model of the gripper is shown in Fig. 11b. Since the clamping force F depends on the position of the tube L_2, the vision algorithm must solve for L_2 in addition to F. Therefore, (17) becomes:

$$E(\theta, X, F, L_2) = \sum_{i=1}^{N} \|r^{i\prime} - w^i\|^2. \quad (19)$$

When this error function is minimized, the force applied to the gripper F and the position of the clamping tube L_2 are found.

5.2 Microgripper Results

A piezoresistive force sensor manufactured by SensorOne (model AE801) was used to verify the output of the vision-based force sensing algorithm. Fig. 12a shows the experimental setup. One jaw of the gripper was applied to the piezoresistive force sensor and the other was applied to a rigid microscrew. The 1 σ precision of the vision algorithm applied to the microgripper was found to be +/- 3.1 mN. The calibration error of the vision algorithm can be seen in Fig. 12c, where output of the vision algorithm, along with the output of the piezoresistive force sensor, is shown versus clamping tube position. The error in this figure is due to errors in the material properties that were assumed for the gripper template. This problem is not particular to vision-based force measurement. With piezoresistive force sensing and laser-based optical force sensing, material properties are also assumed for the object being deformed.

6 Performance Optimizations

As mentioned above, the BFGS method was chosen to minimize the error function. The BFGS method is a gradient-based minimization technique and differs from the steepest descent method in that it uses information from previous iterations in the choice of a new search direction giving it faster convergence rates. BFGS uses information from previous iterations to approximate the Hessian matrix giving it convergence rates similar to second-order minimization techniques without the overhead of computing a second derivative.

Minimizing an error function with any gradient-based minimization technique requires repeated evaluations of the error function and the error function's derivative. For this reason, the minimization process occurs faster if the evaluation of the error function is less computationally expensive. The error function (12) is computationally expensive because, for each template vertex, it is necessary to locate the image vertex that is nearest to it. This problem is known as the nearest-neighbor search or the post office problem. In the simplest solution to the problem, one simply calculates the distance to every image vertex. However, if the image vertex data is organized in a spatial data structure, the nearest image pixel can be found without having to measure the distance to every image pixel. The data structure employed to organize the pixel data is the KD-Tree [11]. A KD-Tree can find the nearest image vertex with $O(logN)$ operations as opposed to $O(N)$ operations required to find the nearest pixel without using a spatial data structure, where N is the number of vertex points in the image.

The performance of the force sensing algorithm was evaluated on an Intel based 2.2 GHz computer with 256 Mb of RAM. The performance of the algorithm is highly dependent on the number of pixels in the template, the number of edge pixels in the image region being passed to the

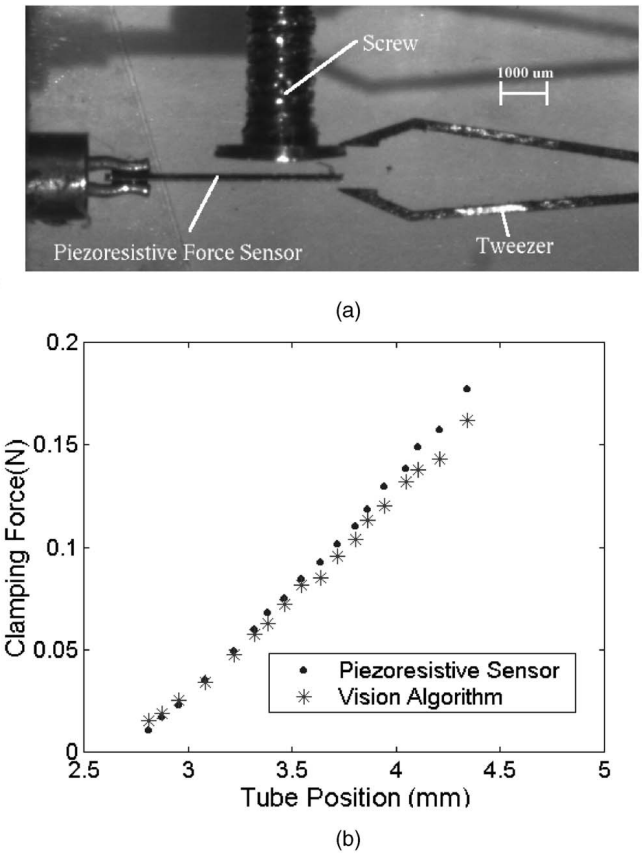

Fig. 12. (a) Micrograpper experimental setup and (b) micrograpper results.

VBFM algorithm, and the shape of the template. For a cantilever beam template with 184 pixels and an input image of approximately 1,000 edge pixels, the VBFM algorithm is able to sustain 30 Hz performance. The achievable performance is reduced to 3 Hz if the KD-Tree data structure is not used to optimize the nearest neighbor search.

7 Conclusions

We have presented a method to reliably measure the force applied to an elastic object through the use of computer vision. It was shown that, through the application of the Dirichlet to Neumann map, the vision-based force measurement problem can be reduced to that of measuring the displacement field of the contour of a deformed object. This observation is important because it shows that boundary data is sufficient to completely recover the force applied to a linearly elastic object independent of object geometry. For nonlinear problems, the Dirichlet to Neumann map can often be modeled numerically and the force measurement problem can be solved using the approach presented in this paper. In addition, performance optimizations were applied to VBFM to achieve real-time performance (30 Hz), making this technique useful for control applications.

Microassembly and biomanipulation require force sensing for success. VBFM provides a means to measure forces through the use of an elastic object. In the two examples given here, the cantilever and the micrograpper, the objects were not initially designed to be used with VBFM; however, they were successfully used as force sensors with no alterations. For the cantilever, sensor resolution of +/- 2.8 nN was achieved, while, for the micrograpper, a resolution of +/- 3.1 mN was demonstrated. These specifications approach resolutions that are achievable with piezoresistive transducers.

Acknowledgments

This research was supported in part by the US National Science Foundation through grant numbers IIS-9996061 and IIS-0208564. Michael Greminger is supported by the Computational Science Graduate Fellowship (CSGF) from the US Department of Energy.

References

[1] J. Canny, "A Computational Approach to Edge Detection," *IEEE Trans. Pattern Analysis and Machine Intelligence,* vol. 8, no. 6, Nov. 1986.
[2] G. Danuser and E. Mazza, "Observing Deformations of 20 Nanometer with a Low Numerical Aperture Light Microscope," *Optical Inspection and Micromeasurements,* vol. 2782, pp. 180-191, 1996.
[3] L. Dong, F. Arai, and T. Fukuda, "3D Nanorobotic Manipulations of Multi-Walled Carbon Nanotubes," *Proc. 2001 IEEE Int'l Conf. Robotics and Automation,* May 2001.
[4] R.B. Guenther and J.W. Lee, *Partial Differential Equations of Math. Physics and Integral Equations.* Englewood Cliffs, N.J.: Prentice Hall, 1988.
[5] M. Kaneko, N. Nanayama, and T. Tsuji, "Vision-Based Active Sensor Using a Flexible Beam," *IEEE/ASME Trans. Mechatronics,* vol. 6, no. 1, pp. 7-16, Mar. 2001.
[6] M. Kass, A. Witkin, and D. Terzopoulos, "Snakes: Active Contour Models," *Int'l J. Computer Vision,* pp. 321-331, 1988.
[7] R.J. Knops and L.E. Payne, *Uniqueness Theorems in Linear Elasticity.* Berlin, Heidelberg: Springer-Verlag 1971.
[8] D. Metaxas, *Physics-Based Deformable Models.* Boston: Kluwer Academic, 1997.
[9] G. Nakamura and G. Uhlmann, "Identification of Lamé Parameters by Boundary Measurements," *Am. J. Math.,* vol. 115, pp. 1161-1187, 1993.
[10] B. Nelson, Y. Zhou, and B. Vikramaditya, "Sensor-Based Microassembly of Hybrid MEMS Devices," *IEEE Control Systems,* Dec. 1998.
[11] H. Samet, *The Design and Analysis of Spatial Data Structures.* Reading, Mass: Addison-Wesley, 1990.
[12] I. Sokolnikoff, *Mathematical Theory of Elasticity.* Malabar, Fla.: Krieger Publishing, 1983.
[13] J. Sylvester and G. Uhlmann, "The Dirichlet to Neumann Map and Applications," *Inverse Problems in Partial Differential Equations,* D. Colton, R. Ewing, W. Rundell, eds., pp. 101-139, 1990.
[14] M. Tortonese, H. Yamada, R.C. Barrett, and C.F. Quate, "Atomic Force Microscopy Using a Piezoresistive Cantilever," *Proc. Transducers '91 Int'l Conf. Solid State Sensors and Actuators,* pp. 448-451, 1991.
[15] T. Tsap, D. Goldgof, and S. Sarkar, "Efficient Nonlinear Finite Element Modeling of Nonrigid Objects via Optimization of Mesh Models," *Computer Vision and Image Understanding,* vol. 69, pp. 330-350, Mar. 1998.
[16] G. Vanderplaats, *Numerical Optimization Techniques for Engineering Design.* New York: McGraw-Hill, 1984.
[17] X. Wang, G.K. Ananthasuresh, and J.P. Ostrowski, "Vision-Based Sensing of Forces in Elastic Objects," *Sensors and Actuators A-Physical,* vol. 94, no. 3, pp. 142-156, Nov. 2001.
[18] G. Yang, J.A. Gaines, and B.J. Nelson, "A Flexible Experimental Workcell for Efficient and Reliable Wafer-Level 3D Microassembly," *Proc. 2001 IEEE Int'l Conf. Robotics and Automation,* May 2001.
[19] A. Yuille, D. Cohen, and W. Hallinan, "Feature Extraction from Faces Using Deformable Templates," *Int'l J. Computer Vision,* vol. 8, no. 2, pp. 99-111, 1992.

Michael A. Greminger received the BS and MS degrees in mechanical engineering from the University of Minnesota in 2000 and 2002, respectively. He is now a mechanical engineering PhD student at the University of Minnesota. He is a recipient of the Computational Science Graduate Fellowship (CSGF) from the US Department of Energy. His research interests include the application of material models to computer vision and the robotic manipulation of deformable objects.

Bradley J. Nelson received the BS degree in mechanical engineering from the University of Illinois at Urbana-Champaign in 1984, the MS degree in mechanical engineering from the University of Minnesota in 1987, and the PhD degree in robotics (School of Computer Science) from Carnegie Mellon University in 1995. He became an assistant professor at the University of Illinois at Chicago in 1995 and an associate professor at the University of Minnesota in 1998. He has worked at Honeywell and Motorola and has served as a United States Peace Corps volunteer in Botswana, Africa. Currently, he is a professor of robotics and intelligent systems at the Swiss Federal Institute of Technology (ETH), Zurich and heads the Institute of Robotics and Intelligent Systems. His most recent scientific contributions have been in the area of microrobotics, including efforts in robotic micromanipulation, microassembly, MEMS (sensors and actuators), mechanical manipulation of biological cells and tissue, and nanofabrication. He has also contributed to the fields of visual servoing, force control, sensor integration, and Web-based control and programming of robots. He has been awarded a McKnight Land-Grant Professorship and is a recipient of the US Office of Naval Research Young Investigator Award, the US National Science Foundation Faculty Early Career Development (CAREER) Award, the McKnight Presidential Fellows Award, and the Bronze Tablet. He is a member of the IEEE.